



Nanocrystalline $\text{Ce}_{1-x}\text{Ru}_x\text{O}_2$ – Microstructure, stability and activity in CO and soot oxidation



M. Kurnatowska^a, W. Mista^a, P. Mazur^b, L. Kepinski^{a,*}

^a Institute of Low Temperature and Structure Research, Polish Academy of Sciences, Okolina 2, 52-422 Wrocław, Poland

^b Institute of Experimental Physics, University of Wrocław, M. Born sq. 9, 50-204 Wrocław, Poland

ARTICLE INFO

Article history:

Received 6 August 2013

Received in revised form 21 October 2013

Accepted 23 October 2013

Available online 30 October 2013

Keywords:

Ce–Ru–O mixed oxide

Nanocrystalline Ru doped ceria

CO oxidation

Soot combustion

TEM

ABSTRACT

Nanocrystalline (4–5 nm) $\text{Ce}_{1-x}\text{Ru}_x\text{O}_2$ mixed oxides ($x=0.03–0.16$) were synthesized using water in oil microemulsion method. Morphology, microstructure and a phase composition of the samples subjected to heat treatment in oxidizing and reducing atmosphere were investigated by TEM, SEM-EDS-EBSD, XRD and XPS. Oxide with $x=0.11$ was structurally stable in oxidizing atmosphere up to 550 °C but above this temperature it decomposed into Ru deficient, nanosized $\text{Ce}_{1-x}\text{Ru}_x\text{O}_2$ and large (few μm) RuO_2 crystals. No phase separation was observed for $\text{Ce}_{0.97}\text{Ru}_{0.03}\text{O}_2$ even after heating at 800 °C. Doping with Ru decreases the size of ceria particles and strongly hinders their sintering at high temperatures. In hydrogen atmosphere a segregation of small (~1 nm) Ru crystallites occurred at the surface of the $\text{Ce}_{0.89}\text{Ru}_{0.11}\text{O}_2$ mixed oxide. Only small increase of the mean crystallite size of Ru (to 2 nm) occurred after reduction at 1000 °C. The unique resistance of Ru to sintering is assigned to a special epitaxial orientation Ru (002)|| CeO_2 (111), which persisted up to the highest temperature of reduction, due to very strong surface bonding. Contrary to a situation in oxidizing atmosphere, doping with Ru had no significant effect on the sintering of ceria in hydrogen. Partial substitution of Ru for Ce strongly enhances the reducibility of ceria at low temperatures and its activity in catalytic combustion of CO and soot.

© 2013 Elsevier B.V. All rights reserved.

1. Introduction

Mixed oxides $\text{Ce}_{1-x}\text{NM}_x\text{O}_{2-y}$ (NM-noble metal) are intensively studied because of their unique properties [1–3]. Doping of ceria with a noble metal enhances its reducibility and thus improves activity as an oxidation catalyst at low temperatures [2,4,5]. Detailed understanding of the behavior of ceria doped with NM is crucial for successful design of new compounds, which could be effective in many fields.

Ruthenium catalysts supported on or promoted with ceria are particularly active in reactions of WAO (wet air oxidation) of organic pollutants [6–9] and hydrogenation of CO_2 [10]. Ceria has a particular role in transporting gas phase oxygen to the metal sites [11,12] and promoting desirable dispersion of Ru on the surface [9]. Low temperature activity of Ru/CeO_2 in oxidizing reactions was assigned to the presence of Ru–O–Ce bonds, which are unstable and can be easily reduced [12]. The Ru–O–Ce groups may be generated alternatively by a partial substitution of Ru ions for Ce^{4+} in CeO_2 lattice. $\text{Ce}_{1-x}\text{Ru}_x\text{O}_{2-y}$ mixed oxides were prepared

by hydrothermal [13] or combustion [14] methods and as thin films by a physical vapor deposition [5]. Maximum doping of Ru in ceria lattice was estimated as $x=0.11$ in the oxide obtained by the hydrothermal method [13]. The mixed oxide showed high activity in WGS (water gas shift) [15], TWC (three way catalysis) [13] and methanation of CO [14] reactions. High activity and stability of $\text{Ce}_{0.9}\text{Ru}_{0.1}\text{O}_{1.94}$ in reducing atmosphere up to 500 °C were observed and ascribed to interesting redox couples: $\text{Ce}^{4+}–\text{Ce}^{3+}$ and $\text{Ru}^{4+}–\text{Ru}^{3+}$ [13]. Chen [16] showed, using DFT + U calculations, that incorporation of Ru ions as substitution point defects into CeO_2 facilitates the formation of oxygen vacancies and thus promotes CO oxidation. The reaction mechanism involves adsorption of molecular oxygen at the oxygen vacancy, formation of O species oxidizing CO, and recovering the stoichiometric surface composition.

This work presents results of the first systematic study of a highly dispersed $\text{Ce}_{1-x}\text{Ru}_x\text{O}_2$ mixed oxide ($x=0–0.2$) prepared by a microemulsion method. The aim was to synthesize a range of nanocrystalline, homogeneous, single phase solid solutions with fluorite structure of CeO_2 and then characterize their structural and chemical properties. The microemulsion method is unique, because it enables to produce uniform complex ceria particles with narrow size distribution in the “true” nanometric range below 10 nm. Microstructure and thermal stability of the oxides in oxidizing, reducing and inert atmospheres over a wide range of temperatures were studied using XRD, TEM, SEM-EDS-EBSD and XPS methods.

* Corresponding author at: Institute of Low Temperature and Structure Research, Polish Academy of Sciences, P.O. Box 1410, 50-950 Wrocław, Poland. Tel.: +48 71 343 50 21; fax: +48 71 344 10 29.

E-mail address: L.Kepinski@int.pan.wroc.pl (L. Kepinski).

Reactivity of the samples was checked by H₂-TPR and combustion of CO and soot as test reactions.

2. Experimental

2.1. Sample preparation

Nanosized Ce_{1-x}Ru_xO₂ mixed oxide was synthesized by water in oil microemulsion method [17]. Triton X-100 was used as a non-ionic surfactant and cyclohexane and 1-pentanol as an organic phase. Water phase containing a solution of cerium and ruthenium nitrates was poured into the organic phase and stirred until a transparent emulsion was obtained. Then the second reactant tetramethylammonium hydroxide (25% water solution) was added and the microemulsion was stirred for 30 min. The organic phase was removed by decanting and the precipitated oxide was washed with acetone (twice) and with methanol (four times). Finally, the solid was separated by centrifugation. All powder samples were dried and heated in oxygen at 500 °C for 2 h. 3 and 8 wt.% Ru/CeO₂ were also prepared, as a reference samples, by an impregnation of a nanocrystalline ceria (prepared using the microemulsion method) with a THF solution of ruthenium trisacetylacetone to incipient wetness, followed by drying at 60 °C and calcination at 300 °C for 1 h [12]. RuO₂ was prepared by simple precipitation: to 0.1 M RuCl₃ aqueous solution an aqueous solution of NaOH was added drop-wise with continuous stirring to obtain precipitation (at pH ~7). The solid precipitate was washed, dried and calcined at 300 °C. A physical mixture of nanocrystalline RuO₂ and CeO₂ (1:1, w/w) was used as a reference sample for XPS study.

2.2. Methods of characterization

Morphology, microstructure and composition of the samples were investigated by TEM (Philips CM20 SuperTwin at 200 kV), TEM/STEM (Philips CM200 FEG at 200 kV with EDS spectrometer EDAX Genesis 4000), SEM-EDS (EDAX Pegasus XM4 spectrometer installed on FEI NovaNanoSEM 230) and XRD (Powder Diffractometer PANalytical using CuKα radiation in the 2θ range 10–110°). The analysis of HRTEM images was made with Digital Micrograph program (Gatan) and XRD patterns were refined using X'Pert High-Score Plus program by Rietveld method. Surface area measurement S_{BET} was performed by the multipoint Brunauer–Emmet–Teller method (BET) with Sorptomatic 1900 FISONS instrument. Nitrogen sorption isotherms were obtained at liquid nitrogen temperature using a volumetric technique on samples out-gassed in a vacuum at 200 °C for 10 h. The total pore volume (V_p) was derived from the amount of nitrogen adsorbed at a relative pressure close to unity (P/P⁰ = 0.98) by assuming that all the accessible pores were then filled with liquid nitrogen. Pore size distribution and a mean pore diameter (D_p) for mesopores was calculated from N₂-desorption isotherm by Barrett–Joyner–Halenda (BJH) method.

XPS spectra were collected with the XPS analyzer Phoibos 100 (SPECS GMBH) equipped with Mg Kα (1253.6 eV) and Al Kα (1486.6 eV) X-ray sources (XR-50 SPEC). In addition to a survey spectrum, detailed scans (a pass energy of 10 eV) of the O(1s), Ru(3d)C(1s), Ru(3p), and Ce(3d) regions were acquired for each sample. Due to a strong overlapping of C(1s) and Ru(3d) lines the XPS spectra were calibrated to yield the value of 916.7 eV for the U'' line in the Ce(3d) band (cf. Fig. 3) [18]. Such calibration procedure has been shown to be appropriate for the samples containing CeO₂ [19]. The powder samples pressed into discs of 8 mm diameter were mounted onto XPS holder using double side carbon tape.

H₂-TPR (temperature programmed reduction) was performed by heating the sample with the heating rate of 10 °C/min up to 900 °C in H₂ (5 vol.%)/Ar flow. The hydrogen consumption was

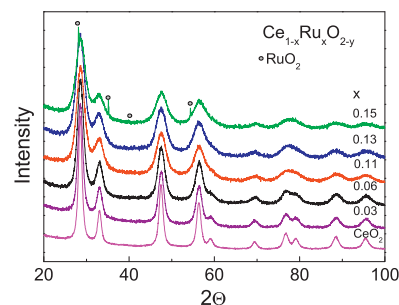


Fig. 1. XRD patterns of "as prepared" Ce_{1-x}Ru_xO₂ ($x = 0\text{--}0.15$) samples.

monitored by thermo-conductivity (TCD) detector. Before TPR the samples were shortly heated in O₂ (1%)/He at 500 °C (ceria and mixed oxide) or 300 °C (Ru/CeO₂) to clean the surface. After the first TPR run, the samples were oxidized at 500 °C (with TPO being recorded) and then were cleaned with pure He at room temperature.

2.3. Catalytic tests

A catalytic reaction test for CO oxidation was carried out at atmospheric pressure in a flow U-shaped quartz tube reactor of 4 mm internal diameter and 20 cm length. The catalyst bed (0.150 g) was heated from –20 °C to 100 °C at constant rate of 3 °C/min while supplying a gas mixture containing CO (1%) in an artificial air (20% O₂/80% N₂) flowing at 75 ml/min. The effluent gas (CO, O₂ and CO₂) was analyzed by the on-line mass spectrometer (OmniStar QMS-200).

Combustion of a model soot (a carbon black Printex-U from Degussa S.A) was performed by heating a soot–catalyst mixture in air in TG analyzer (Derivatograph MOM Q-1500D). The samples were prepared in "tight contact" mode by grinding a mixture of the catalyst (ca. 80 mg) and the soot (catalyst/soot = 2:1 by weight) in an agate mortar.

3. Results and discussion

3.1. Structure characterization

3.1.1. Fresh samples

Multi-point EDS analyses of all "as prepared" samples were performed to check the homogeneity of the samples. The measured Ru contents ($x = 0.03, 0.06, 0.11, 0.13$ and 0.15) were close to the nominal ones (0.03, 0.05, 0.1, 0.125 and 0.15). For all samples, deviations of the composition from the mean value were at various points around 0.02 (which is consistent with accuracy of measurement).

The nitrogen adsorption/desorption isotherm and pore size distribution of a representative Ce_{0.89}Ru_{0.11}O₂ sample are shown in Fig. S1 (supporting information). The sample exhibits the classical shape of a type IV isotherm according to the IUPAC classification, typical for mesoporous solids. The pore size distribution (inset to Fig. S1) indicates a mesoporous structure and confirms a relatively narrow distribution of pore sizes. The BET surface area, average pore diameter (D_p) and pore volume for the Ce_{0.89}Ru_{0.11}O₂ sample were 124 m²/g, 3.6 nm and 0.113 cm³/g, respectively. The average particle size of 7 nm, evaluated from BET data using the formula $d_{av} = 6000/(\rho S_{BET})$, where $\rho = 6.94$ [g/cm³]—density of the oxide, is 60% bigger than mean crystallite size of 4 nm obtained from XRD and TEM (Table 1). The reason is agglomeration of the crystallites seen in TEM micrographs (Fig. 2b).

XRD patterns revealed (Fig. 1) that up to $x = 0.13$ the "as prepared" samples contain exclusively reflections of fluorite type structure of CeO₂. For $x = 0.15$ sharp reflections of RuO₂ were

Table 1XRD and TEM characterization of the “as prepared” $\text{Ce}_{1-x}\text{Ru}_x\text{O}_2$ samples.

Sample	a [nm]	Size [nm] XRD	Microstrain %	Oxygen occupancy	Size [nm] TEM	Second phase
$x=0$	0.54115 (3)	8.6	0.26	1	8.6	
$x=0.03$	0.54079 (4)	6.5	0.43	1	6.2	
$x=0.06$	0.54060 (5)	5.4	0.64	1	5	
$x=0.11$	0.5411 (1)	4.3	0.88	0.987	3.9	
$x=0.13$	0.5411 (2)	4	0.86	0.97	3.7	
$x=0.15$	0.5411 (2)	3.7	0.77	0.98	3.7	RuO_2 1.4%

additionally observed (Fig. 1). Macroscopic phase separation and formation of large RuO_2 crystals (few μm) in $\text{Ce}_{0.85}\text{Ru}_{0.15}\text{O}_2$ were confirmed by SEM-EDS (Fig. 2a) and EBSD (Fig. S2 in supporting information). It cannot be excluded however, that the $\text{Ce}_{0.85}\text{Ru}_{0.15}\text{O}_2$ sample was homogeneous after synthesis but then decomposed partially into the mixed phase and ruthenium oxide during calcination at 500 °C. Structure parameters (lattice parameter, mean crystallite size, microstrain and oxygen occupancy) were derived from the XRD patterns using Rietveld refinement method and are presented in Table 1. The lattice parameters of all samples were similar and no systematic change with Ru content occurred. Such behavior differs from that observed previously for Rh and Pd doped nanocrystalline ceria [21,22], where the lattice parameter increased with the metal content. The reason is relatively small ionic radius of Ru^{4+} (62 pm), which compensates the expansion of the lattice of ceria caused by decreasing crystallite size due to doping with Ru. Singh et al. [13] observed a slight increase of the lattice parameter of $\text{Ce}_{1-x}\text{Ru}_x\text{O}_{2-y}$ ($x=0.05-0.1$) comparing to pure CeO_2 . The authors suggested that even though Ru ion is significantly smaller than Ce^{4+} , the presence of Ce^{3+} ions and oxygen vacancies caused the resultant increase of the lattice parameter. As appears from Table 1, a microstrain increases with increasing x and then slightly decreases when the sample becomes biphasic ($x=0.15$). Such behavior indicates, that the microstrain attains a maximum for the concentration of the dopant close to the saturation. An oxygen occupancy for $\text{Ce}_{0.89}\text{Ru}_{0.11}\text{O}_2$ was 0.987, very close to that of CeO_2 indicating that Ru enters ceria lattice probably as +4 ion, isovalent to Ce (cf. XPS data below).

Fig. 2b presents typical HRTEM image of the “as prepared” $\text{Ce}_{0.89}\text{Ru}_{0.11}\text{O}_2$ sample. The crystallites exhibit well developed faces and have a narrow size distribution (inset to Fig. 2b) with a mean value of ~4 nm. This value is consistent with that obtained from Rietveld refinement of XRD data (Table 1). Similar, good correspondence between XRD and TEM occurred for other “as prepared” samples (Table 1). It is seen that the mean size of the crystallites

decreases with increasing amount of Ru dopant. The same effect was observed for Pd and Rh doped ceria [21,22]. Contrary, Singh et al. [13] observed an increase of the mean crystallite size of ceria with Ru addition, 6.9 nm and 10.7 nm for $x=0.05$ and $x=0.1$, respectively.

Three samples: $\text{Ce}_{0.89}\text{Ru}_{0.11}\text{O}_2$, 3% Ru/ CeO_2 , and $\text{CeO}_2 + \text{RuO}_2$ (1:1, w/w physical mixture) were studied by XPS. Fig. 3a shows a survey XPS spectrum of $\text{Ce}_{0.89}\text{Ru}_{0.11}\text{O}_2$ acquired using Al K α radiation. The most important lines discussed in the paper are marked. Carbon was the only contamination identified in all samples, except for $\text{CeO}_2 + \text{RuO}_2$, where Na was also detected. The origin of Na contamination is NaOH used in the synthesis of RuO_2 . As it will be discussed later the carbon exists as an adventitious carbon – peak at 284.8 eV (C1 in Fig. 4e) and as carbonate groups adsorbed at the surface of ceria – peak at 288.8 eV (C2 in Fig. 4e).

Figs. 3(b and c) and 4 show XPS high resolution spectra of Ce(3d), O(1s), Ru(3d)C(1s) and Ru(3p) regions. Most important data retrieved from the XPS spectra are given in Table 2. Peak parameters (position of the maximum, peak width (FWHM) and intensity) were extracted from the high resolution spectra after background subtraction (Shirley or Shirley + linear type) by fitting procedure applied in XPSPEAK.41 program [23]. Quantitative information on the composition of the samples (Table 3) was extracted from the XPS spectra on assumption of a homogeneous distribution of the elements (homogeneous model). This assumption is clearly not valid for the samples studied (except the $\text{Ce}_{0.89}\text{Ru}_{0.11}\text{O}_2$) but complex morphology of the samples would require application of advanced models, which is beyond the scope of this work. The quantitative results presented in this work must be considered therefore only as indications of differences between the samples. Relative sensitivity factors, taking into account the escape depth and geometry of the spectrometer, were provided by the producer of the spectrometer: O(1s) – 4.211; Ru(3p_{3/2}) – 8.738; Ce(3d) – 37.873. Using data in Table 3 we obtain for the $\text{Ce}_{0.89}\text{Ru}_{0.11}\text{O}_2$ a value of x in the $\text{Ce}_{1-x}\text{Ru}_x\text{O}_2$ equal to 0.12, which is close to the

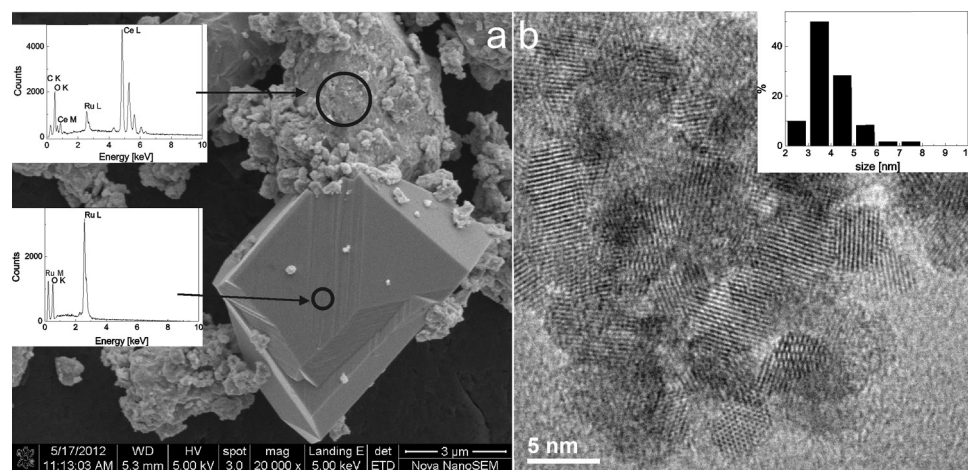


Fig. 2. (a) SEM image of “as prepared” $\text{Ce}_{0.85}\text{Ru}_{0.15}\text{O}_2$ sample with EDS spectra at pointed areas (insets). (b) HRTEM image and crystallite size distribution (inset) of “as prepared” $\text{Ce}_{0.89}\text{Ru}_{0.11}\text{O}_2$.

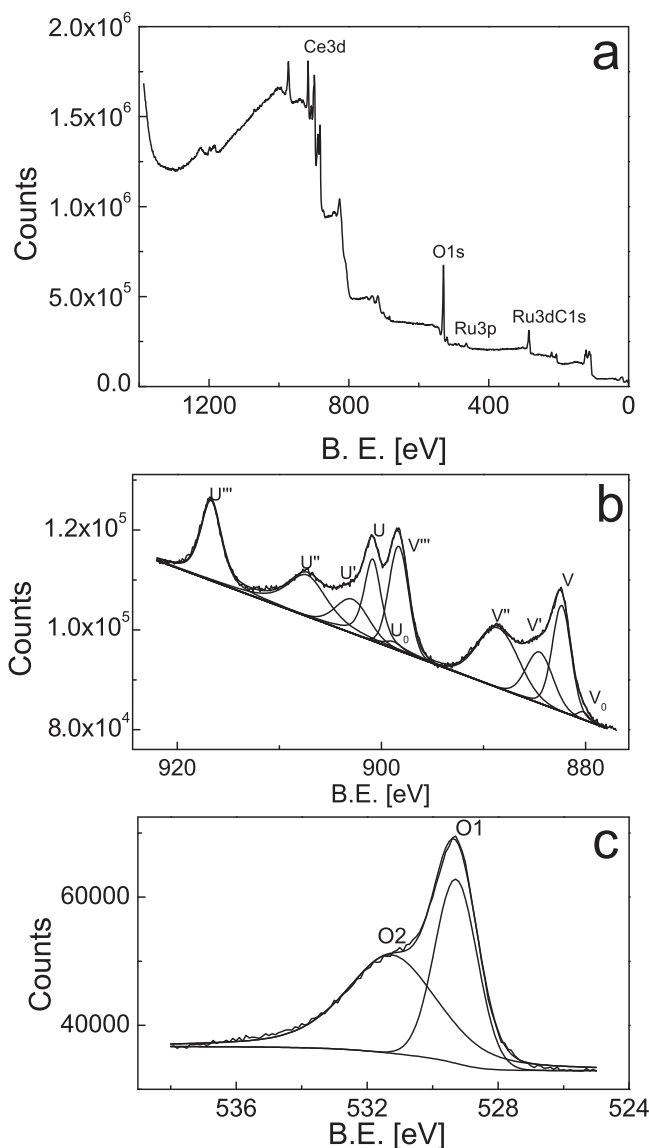


Fig. 3. XPS spectra: (a) survey spectrum of $\text{Ce}_{0.89}\text{Ru}_{0.11}\text{O}_2$ sample, (b) Ce(3d) and (c) O(1s) high resolution spectra of $\text{CeO}_2 + \text{RuO}_2$.

value of 0.11 measured by EDS. This indicates that the sample is homogeneous with no segregation of Ru at the surface of the mixed oxide. Ce(3d) spectra of all samples were very similar so only representative example obtained for $\text{CeO}_2 + \text{RuO}_2$ is shown (Fig. 3b). The spectrum shows good correspondence with reference spectra of nanocrystalline CeO_2 [18] and indicates that most of the Ce exists as Ce^{4+} ions with only small addition of Ce^{3+} ions ($\text{V}^0, \text{V}', \text{U}^0, \text{U}'$ lines). It is worth mentioning that U'' line is related exclusively with Ce^{4+} ions and its position is not affected by the presence of Ce^{3+} [18]. Therefore, it can be used as a good reference for in situ energy scale calibration. The presence of $\sim 16\%$ of Ce^{3+} in the $\text{CeO}_2 + \text{RuO}_2$ sample (Table 3) is the result of small size of ceria crystallites (the presence of not fully coordinated Ce ions at the surface) and the effect of reduction induced by X-rays in XPS spectrometer [24]. The estimation of Ce^{3+} content in the samples (Table 3) is very rough. Ce^{3+} ions may occur as the result of small size of ceria crystallites (the presence of not fully coordinated Ce ions at the surface), due to doping with aliovalent ions but also due to reduction induced by X-rays in XPS spectrometer [24]. Low Ce^{3+} content in the $\text{Ce}_{0.89}\text{Ru}_{0.11}\text{O}_2$ may indicate that Ru exists in the ceria lattice as isostructural Ru^{4+} additive, which does not generate intrinsic oxygen vacancies.

The chemical state of Ru in the samples was determined by the analysis of Ru(3d_{5/2}) and Ru(3p_{3/2}) lines. The former is more intense and more suitable for study of energy shifts but there is a problem of its overlapping with C(1s) line, often present in the spectra. Therefore, Ru(3p_{3/2}) line was also evaluated, especially for quantitative analysis. Ru(3d_{5/2}) line of $\text{CeO}_2 + \text{RuO}_2$ sample contains two components at 280.7 eV and 282.1 eV (Fig. 4e). The former fits well the position reported in literature for crystalline RuO_2 [25], but also for thin RuO_2 films and thin layers formed at the surface of metallic Ru [26,27]. The latter is identified in literature as a characteristic satellite feature in RuO_2 due to plasmon losses [28], unscreened Ru^{4+} cations [29,30] or RuO_x oxide with Ru at oxidation state higher than 4+ [31,32]. Though there is still a debate on the origin of the high energy satellite in the Ru(3d_{5/2}) line of RuO_2 , the electronic origin (unscreened final state) seems to be the most appropriate [33]. The complex structure of Ru(3d_{5/2}) line is also reflected in Ru(3p_{3/2}) line (Fig. 4a), where the main component at 462.6 eV corresponds to Ru^{4+} in RuO_2 and the second feature at 465.5 eV is a final state satellite [34]. O(1s) spectrum of the $\text{CeO}_2 + \text{RuO}_2$ sample (Fig. 3c) shows two components: a narrow one at 529.3 eV and broad one at 531.2 eV. The first feature is a composition of two close lying lines from RuO_2 (529.4 eV [35]) and CeO_2 (529.6 eV [18]). The broad feature at 531.2 eV is a complex line from various species (OH, CO_3) adsorbed at the surface. The O(1s) spectra of other samples were similar and are not presented. The Ru(3d_{5/2}) line of the $\text{Ce}_{0.89}\text{Ru}_{0.11}\text{O}_2$ (Fig. 4f) differs strongly from that of $\text{CeO}_2 + \text{RuO}_2$ since it contains only one component at 282.3 eV and similarly, only a single 3(p_{3/2}) line at 463.4 eV (Fig. 4b). It is interesting that both lines occur at energies much higher than those of RuO_2 , indicating that electronic structure (or environment) of the Ru ions is different. The presence of a single line proves also that distribution of Ru in the sample is homogeneous with no noticeable segregation of Ru at the surface as separate RuO_2 phase. Singh and Hegde [13] studied $\text{Ce}_{0.95}\text{Ru}_{0.05}\text{O}_{2-\delta}$ and $\text{Ce}_{0.90}\text{Ru}_{0.10}\text{O}_{2-\delta}$ mixed oxides prepared by hydrothermal synthesis and in both observed the Ru(3d_{5/2}) line at 281.4 eV and the Ru(3p_{3/2}) peak at 463.1 eV, i.e., at higher BE than in RuO_2 . Similarly, Sharma et al. [14] and Shinde and Madras [36] reported the position of Ru(3p_{3/2}) line at 463.1 eV in $\text{Ce}_{0.95}\text{Ru}_{0.05}\text{O}_2$ and $\text{Ce}_{0.85}\text{M}_{0.1}\text{Ru}_{0.05}\text{O}_2$ ($\text{M} = \text{Si}, \text{Fe}$) mixed oxide prepared by combustion and sonochemical method, respectively. There is an open question on the reason for the high energy shift of Ru(3d) and Ru(3p) lines in the mixed oxides. Singh and Hedge [13] stated that binding energy for Ru3d_{5/2} in $\text{Ce}_{0.90}\text{Ru}_{0.10}\text{O}_2$ agrees well with the binding energy value for Ru^{4+} ion in $\text{RuO}_2 \text{xH}_2\text{O}$ and thus Ru is in the +4 state. According to [14,36] the difference in the environment of Ru ions in RuO_2 and in ceria results in energy shift but in both cases a formal charge of Ru is 4+. Ru^{4+} ions in RuO_2 occupy a single site being coordinated with 6 O ions and a coordination polyhedron is a square bipiramid with 4 Ru–O distances of 0.19857 nm and 2 shorter distances 0.19414 nm [37]. It differs strongly from the VIII coordination of Ce^{4+} in CeO_2 with 8 Ce–O distances of 0.2343 nm, so that observed shift in the binding energy of Ru(3d) and Ru(3p) lines for Ru occupying a Ce site in ceria lattice is possible. XPS Ru(3d_{5/2}) spectrum of 3 wt.% Ru/ CeO_2 sample prepared by impregnation, containing two components at 280.9 and 282.0 eV (Fig. 4h), resembles that of $\text{CeO}_2 + \text{RuO}_2$ sample indicating the presence of RuO_2 . Ru(3p_{3/2}) line (Fig. 4d) also contains two components at 462.5 and 463.7 eV.

3.1.2. Heating in oxidizing or inert atmosphere

Fig. 5 presents XRD patterns of $\text{Ce}_{0.89}\text{Ru}_{0.11}\text{O}_2$ heated in oxygen at 600 °C (a) and at 800 °C (c) and in argon at 700 °C (b). For comparison the patterns of 8 wt.% Ru/ CeO_2 (d), 3 wt.% Ru/ CeO_2 (e) and $\text{Ce}_{0.97}\text{Ru}_{0.03}\text{O}_2$ (f) heated at 800 °C in oxygen are also shown. For $\text{Ce}_{0.89}\text{Ru}_{0.11}\text{O}_2$, weak, but very sharp reflections of RuO_2 became visible already after heating at 600 °C for 2 h (Fig. 5a).

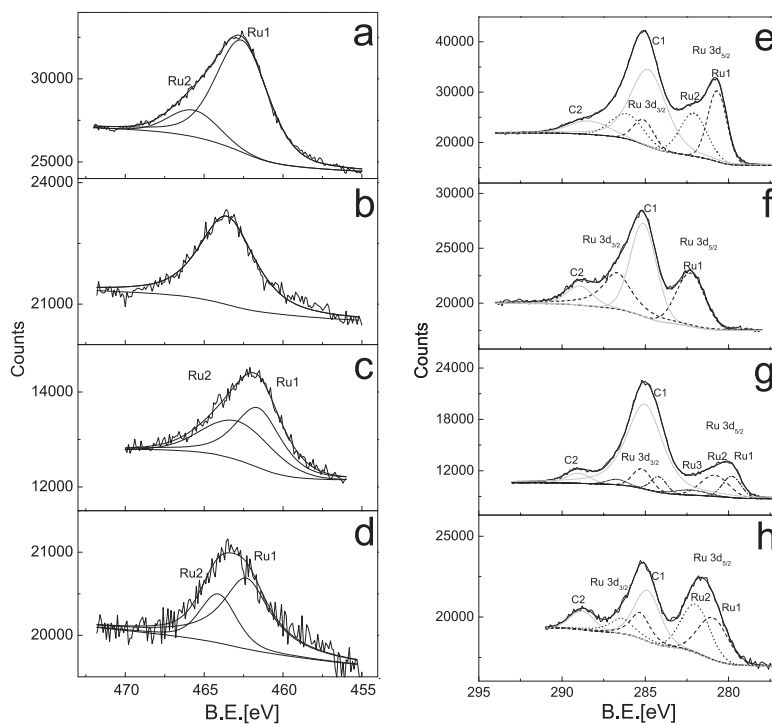


Fig. 4. High resolution Ru(3d) (a–d) and Ru(3p) (e–h) XPS spectra of CeO₂ + RuO₂ (a, e), “as prepared” Ce_{0.89}Ru_{0.11}O₂ (b, f), Ce_{0.89}Ru_{0.11}O₂ reduced at 800 °C (c, g) and Ru/CeO₂ (d, h).

It indicates a phase separation with formation of rare but rather large crystallites of RuO₂, similar as it was observed before for Ce_{1-x}Rh_xO_{2-y} [22]. Refinement of the XRD pattern revealed that crystalline RuO₂ constitutes 4.5 wt.% of the sample, slightly more than half of total 8 wt.% of RuO₂ formerly present in the “as prepared” Ce_{0.89}Ru_{0.11}O₂ (Table 4). SEM-EDS and TEM confirmed this suggestion revealing the presence of large, well develop RuO₂ crystals (up to ~15 μm) mixed with nanosized ceria containing ~3.5% of Ru (Fig. 6). Interestingly, SAED pattern (inset)

contains sharp spots from large RuO₂ crystallite and rings from ceria, with no evidence of additional features from nanocrystalline RuO₂. HRTEM showed that nanocrystalline Ru deficient ceria contains exclusively well-developed particles free from any amorphous or highly dispersed RuO₂ phase. The lack of RuO₂ reflections in the XRD pattern of Ce_{0.97}Ru_{0.03}O₂ treated in oxygen at 800 °C (Fig. 5d) indicates that the weakly doped Ce–Ru–O mixed oxide is stable in oxidizing atmosphere at high temperature.

Table 2
Binding energies (BE), line widths (FWHM) and intensities (*I*) extracted from the high resolution XPS spectra.

Sample	Ru3d _{5/2}			Ru3p _{3/2}			Ce3d _{5/2}			O1s		
	BE [eV]	Δ [eV] ^a	<i>I</i> ^b	BE [eV]	Δ [eV]	<i>I</i>	BE [eV]	Δ [eV]	<i>I</i>	BE [eV]	Δ [eV]	<i>I</i>
CeO ₂ + RuO ₂	280.7 ^h	1.4	20233	462.6 ⁱ	3.7	32315	882.4 ^c	2.3	52761	529.3 ^f	1.5	46652
	282.1 ^j	1.9	17849	465.5 ^k	3.6	6197	884.7 ^d	2.9	31649	531.2 ^g	3.4	64529
	282.3	2.0	10390	463.4	4.1	12429	888.6 ^e	4.9	64954			
Ce _{0.89} Ru _{0.11} O ₂ fresh	282.3	2.0	10390	463.4	4.1	12429	882.4	2.1	89704	529.4	1.4	76341
							884.5	2.7	44560	531.4	2.4	39430
							888.7	4.8	118383			
Ce _{0.89} Ru _{0.11} O ₂ 800 °C H ₂	279.8	1.3	3450	461.7	3.1	4471	882.4	2.4	29912	529.2	1.7	18278
	280.8	2.0	5771	462.9	5.1	5910	884.4	2.5	15028	531.8	3.9	34609
	282.3	1.0	183				888.6	5.3	41600			
3 wt.% Ru/CeO ₂	280.9	2.1	5924	462.3	3.6	4866	882.4	2.1	95393	529.2	1.5	72076
	282.0	2.0	6432	464.1	2.9	1993	884.5	2.7	49821	531.1	2.9	40922
							888.7	4.7	127196			

^a Full width at half maximum (FWHM).

^b Intensity (area under the peak).

^c Line marked V in Fig. 2 – related to Ce⁴⁺ ions.

^d Line marked V' in Fig. 2 – related to Ce³⁺ ions.

^e Line marked V'' in Fig. 2 – related to Ce⁴⁺ ions.

^f Line marked O₁ in Fig. 5.

^g Line marked O₂ in Fig. 5.

^h Line marked Ru₁ in Fig. 3.

ⁱ Line marked Ru₂ in Fig. 3.

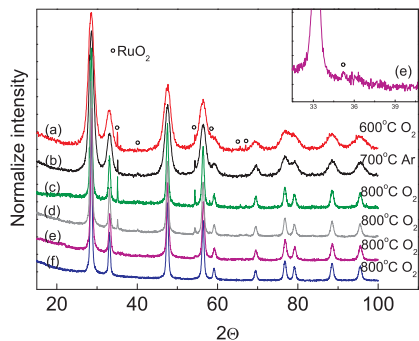
^j Line marked Ru₁ in Fig. 4.

^k Line marked Ru₂ in Fig. 4.

Table 3

Composition of the samples calculated from the XPS spectra.

Sample	Composition [at.%]			[Ce(3+)] ^d
	[Ce] ^a	[Ru] ^b	[O] ^c	
Ce _{0.89} Ru _{0.11} O ₂	34.9	4.7	60.3	9.7
Ce _{0.89} Ru _{0.11} O ₂ 800 °C, H ₂	40.6	12.8	46.3	15
3 wt.% Ru/CeO ₂	39.6	2.6	57.7	12
CeO ₂ + RuO ₂	29.0	20.2	50.8	16.3

^a Calculated using a total intensity of Ce3d lines in Ce3d spectrum.^b Calculated using a sum of Ru₁ and Ru₂ lines in Ru3p spectrum.^c Calculated using O₁ line in O1s spectrum.^d Quantity connected with the content of Ce³⁺ ions in the sample.
[Ce³⁺] = (IU⁰ + IV⁰ + IU' + IV')/(IU⁰ + IV⁰ + IU + IV + IU'' + IV'' + IU''' + IV''').**Fig. 5.** XRD patterns of the samples heated in oxygen or argon: Ce_{0.89}Ru_{0.11}O₂ (a–c), 8 wt.% Ru/CeO₂ (d), 3 wt.% Ru/CeO₂ (e) and Ce_{0.97}Ru_{0.03}O₂ (f).**Table 4**XRD characterization of the Ce_{1-x}Ru_xO₂ heated in oxygen.

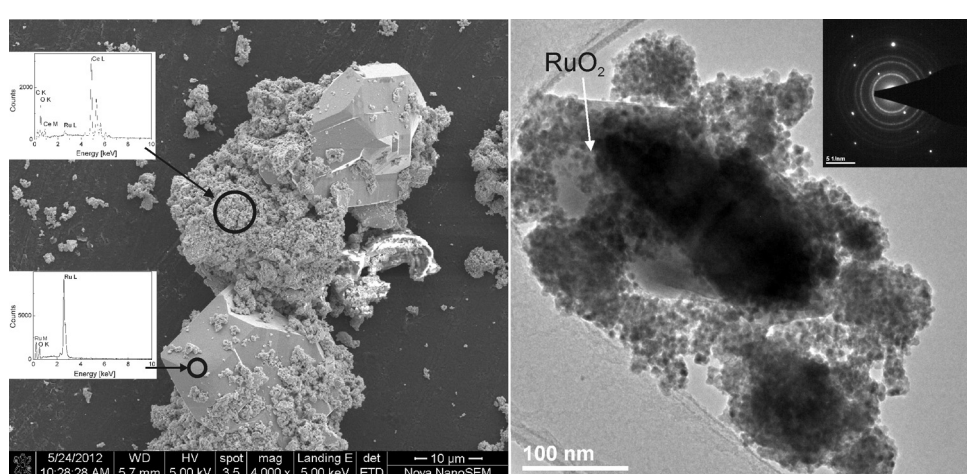
Sample	Treatment	<i>a</i> [nm]	Size [nm]	Second phase
CeO ₂		0.54102 (4)	56	–
Ce _{0.97} Ru _{0.03} O ₂	O ₂ /800 °C	0.54092 (1)	17.5	–
Ce _{0.89} Ru _{0.11} O ₂		0.54095 (2)	16.6	RuO ₂ 4.5 wt.%
Ce _{0.89} Ru _{0.11} O ₂	O ₂ /600 °C	0.54091 (3)	5.1	RuO ₂ 1.2 wt.%
Ce _{0.89} Ru _{0.11} O ₂	Ar/700 °C	0.54076 (2)	6.1	RuO ₂ 1.3 wt.%

In additional experiment a stability of Ce_{0.89}Ru_{0.11}O₂ in an inert atmosphere (argon) was checked. The process of phase separation was similar as in oxygen but started at the temperature about 100 °C higher (Fig. 5b). This means that the presence of gaseous oxygen facilitates the formation of the phase responsible for rapid growth of RuO₂ crystals, but it is not essential. Parameters obtained

from Rietveld refinement of XRD patterns of CeO₂, Ce_{0.89}Ru_{0.11}O₂ and Ce_{0.97}Ru_{0.03}O₂ heated in O₂ and Ar are given in Table 4. The lattice parameter of Ce_{0.89}Ru_{0.11}O₂ heated at 800 °C is very close to that of Ce_{0.97}Ru_{0.03}O₂ and it is smaller than that of pure CeO₂. Moreover, mean crystallite sizes of both doped samples are similar but significantly smaller than the mean crystallite size of CeO₂. These observations indicate that ceria lattice can accommodate at least 3 mol % of Ru in the oxidizing atmosphere at 800 °C. Ru inhibits also crystallite growth of ceria, though the effect is weaker than reported for other metals (Pd, Rh) [21,22]. The reason for the stronger inhibiting effect of Pd and Rh could be higher thermal stability of Pd and Rh doped ceria (no phase separation occurred in Ce_{0.89}Pd_{0.11}O_{2-y} and Ce_{0.89}Rh_{0.11}O_{2-y} in oxidizing atmosphere at 800 °C).

A process of the phase separation in Ce_{0.89}Ru_{0.11}O₂ in air was also investigated by "in situ" XRD from 500 to 800 °C. The sample was heated with a rate 5 °/min to a desired temperature and then XRD pattern was acquired during 30 min. Next, the sample was kept at this temperature for 30 min and the second pattern was collected. The procedure was repeated for all temperatures. First sign of the phase separation was noticed after 30 min heating at 575 °C, when small, but sharp reflection assigned to (101) RuO₂ appeared at 2θ = 35° (Fig. 7a). At 600 °C the intensity of the (101)RuO₂ reflection increased strongly and the process continued at higher temperatures. The RuO₂ reflection is very sharp, so that both Kα1 and Kα2 components are seen. The intensity and shape of RuO₂ reflections in the first and the second pattern acquired at 800 °C were the same, which means that phase separation was already completed. Sintering of the ceria phase started at 575 °C and occurred simultaneously with extraction of Ru from the crystal lattice (Fig. 7). Mean crystallite sizes calculated from the (200) CeO₂ reflection using Scherrer equation were 5.3, 5.6, 6.7, 13.4 and 38 nm at 500, 575, 600, 700 and 800 °C, respectively. Differences in the behavior observed during "in situ" and "ex situ" experiments (e.g., in the onset of phase separation) emerge from different experiment conditions (different total time of heating at given temperature, different oxygen partial pressure).

A mechanism of formation of large RuO₂ crystals during heating of Ce_{0.89}Ru_{0.11}O₂ in oxidizing atmosphere is probably similar to that reported for Ce_{0.89}Rh_{0.11}O₂ [22]. It is assumed that during heating Ru ions segregate at the surface of the mixed oxide and create a mobile Ru–O–Ce phase which allows for a fast mass transport of Ru species and crystallization of large RuO₂ crystals. In line with this, Chen et al., [38] reported that the presence of Ti facilitates the crystallization of RuO₂ nanorod crystallites in an amorphous Ru–Ti mixed oxide.

**Fig. 6.** Morphology of Ce_{0.89}Ru_{0.11}O₂: heated at 800 °C in O₂ – SEM-EDS (a), heated in argon 700 °C – TEM and (b) inset shows SAED pattern.

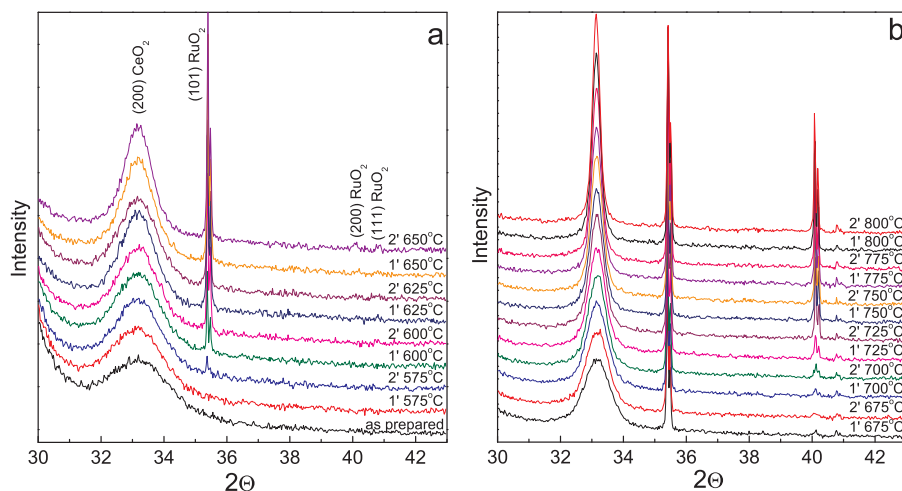


Fig. 7. XRD patterns for Ce_{0.89}Ru_{0.11}O₂ recorded "in situ" during heating in air up to 650 °C (a) and at 675–800 °C (b). First measurement (1') (lasting 30 min) was done immediately after reaching the desire temperature. Second measurement (2') was performed after 30 min heating at the temperature of the first measurement.

For the 3 wt.% Ru/CeO₂ sample prepared by impregnation, no RuO₂ reflections could be seen in XRD pattern. The heating at 800 °C in O₂ caused the formation of very small amount of nanocrystalline RuO₂ (Fig. 5e), indicating that most Ru is present as highly dispersed surface phase. At higher Ru loading, 8 wt.% Ru/CeO₂ (which corresponds to 11 atomic % Ru – the same amount as in Ce_{0.89}Ru_{0.11}O₂), broad RuO₂ reflections could be seen already after treatment at 300 °C but heating at 800 °C in O₂ caused the growth of well developed RuO₂ crystallites, similar, but smaller than those observed in Ce_{0.89}Ru_{0.11}O₂ (Fig. 5d, Fig. S3). The amount of crystalline RuO₂ was estimated as 4.4 wt.%, what suggests that the remaining Ru (~3 wt.% in this case), is a maximum amount which may be dispersed at the surface of ceria as stable Ru–O–Ce phase. Obviously, this maximum amount must depend on the available surface of CeO₂ support. Given S_{BET} of CeO₂ support equal to 62 m²/g, the surface concentration of Ru is 2.8 and 7.6 Ru atoms/nm² for "as prepared" 3 and 8 wt.% Ru/CeO₂, respectively. Growth of the mean crystallite size of ceria from 8.6 to 16 nm after heating at 800 °C caused a decrease of the surface area of the support to 33 m²/g with corresponding increase of the Ru concentration at the surface to 5.4 and 14.3 Ru atoms/nm². It appears therefore that ca. 5 Ru atoms/nm² is involved in Ru–O–Ce surface phase stable at 800 °C in the oxidizing atmosphere. The surplus Ru oxide is only weakly bound with the surface and sinters easily to form large RuO₂ crystallites. For Ce_{0.89}Ru_{0.11}O₂ solid solution, with surface area of 124 m²/g, the surface concentration of Ru may be estimated as 0.9 Ru/nm² (1/9 of Ce concentration at (111) surface of CeO₂ equal to 8 Ce/nm²). Heat treatment at high temperature (above 600 °C) causes a decline of the surface area of ceria and segregation of some Ru at the surface. As the result, maximum capacity of the surface is exceeded and growth of crystalline RuO₂ occurs. In this context it is interesting to recall the work by Satsuma et al. [39], who observed self-dispersion of Ru powder with average crystallite size 36 nm into nanosized particles (not detected by XRD) on a high surface CeO₂ during heating in air at 700 °C. The process was much less effective in N₂ atmosphere, indicating that the oxidation of Ru particles plays an important role in the self-dispersion process. Similarly, the self-dispersion process did not occur on different supports (e.g., MgO, Al₂O₃, SiO₂). The authors concluded therefore, that formation of Ru–O–Ce species at the surface of ceria during calcination was responsible for the dispersion of ruthenium. The Ru–O–Ce phase reduced in hydrogen at 200–400 °C was an active catalyst of CO oxidation [39]. In literature dispersion of MoO₃ and WO₃ deposited onto CeO₂ by impregnation was studied [40,41].

The maximum monolayer capacity of CeO₂ was estimated as 4.2 and 4.8 Me atom/nm², respectively.

3.1.3. Heating in reducing atmosphere

XRD patterns of Ce_{0.89}Ru_{0.11}O₂ after reduction at various temperatures are presented in Fig. 8. The treatment caused sharpening of the oxide reflections, very distinct at 500 °C and gradual at higher temperatures. Moreover, after treatment at 500 °C, the strongest (101) reflection of Ru metal appeared as a very weak, broad peak at ~44°. The peak became narrower after heating at 600 °C but then disappeared at 800 °C (inset to Fig. 8). In order to explain such unexpected behavior a thorough TEM investigations were performed. In harmony with XRD, reduction at 400 °C caused only some growth of the oxide crystallites with no evidence of phase separation (Fig. S4). The crystallites expose well-developed faces with large number of defects (edges and kinks). The morphology of the sample changed at higher temperatures. After heating at 500 °C small, dark particles with an average size of 1.2 nm could be seen on the surface of ceria crystallites (Fig. 9a). No crystal features such as lattice or Moire fringes could be seen, most probably due to very small size of the Ru particles. After reduction at 600 °C the particles grew and their crystalline structure could be observed (Fig. 9b–d). The Ru particles show various orientations relative to underlying ceria crystallites as indicated by arrows in Fig. 9b. Some of them assume preferred epitaxial orientation observed as Moire fringes in plane view (Fig. 9b) or directly in edge view (Fig. 9d). Ru crystallites with structure defects such as stacking faults (an error in a sequence of the layers) could be seen (Fig. 9d). Most of the Ru particles have

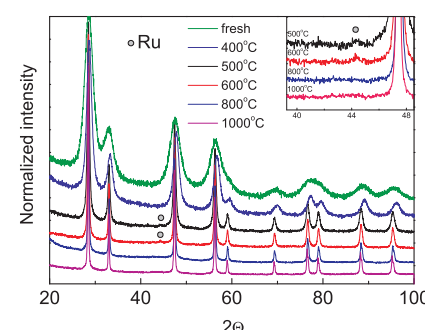


Fig. 8. XRD patterns of Ce_{0.89}Ru_{0.11}O₂ heated in hydrogen at 500 °C, 600 °C, 800 °C and 1000 °C for 1 h. Inset presents zoomed region in the vicinity of Ru (101) reflection.

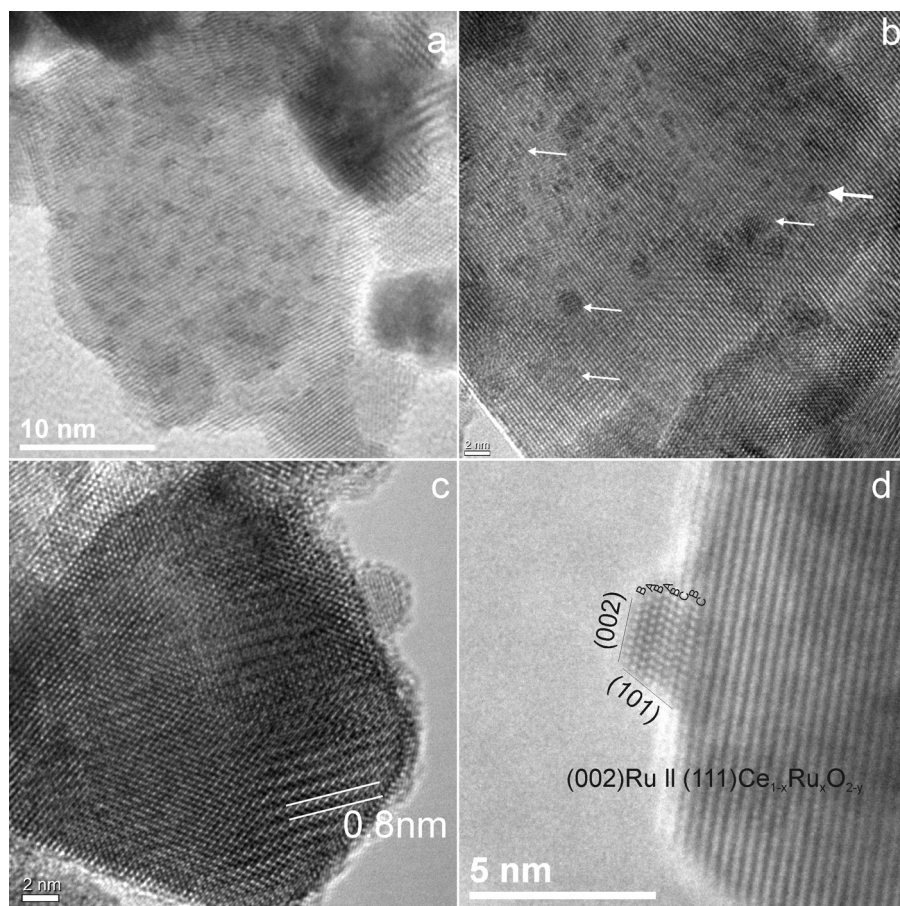


Fig. 9. TEM images of Ce_{0.89}Ru_{0.11}O₂ heated in hydrogen at 500 °C (a) and 600 °C (b–d).

a thin amorphous layer at the surface, probably an oxide formed upon exposure of the reduced samples to air (Fig. 9c).

Increasing the temperature of treatment in hydrogen caused growth of Ru crystallites and their rearrangement on the ceria surface. After reduction at 1000 °C most of the Ru particles assume preferred epitaxial orientation on the support. Fig. 10a shows an example of the particle with parallel Moire fringes which, according to FFT pattern (inset to Fig. 10a), originate from interference of parallel (1 1 1) CeO₂ and (0 0 2) Ru lattice fringes. Hernandez et al. also observed the same epitaxial relationship for Ru supported on ceria [42]. The shape of the particle in Fig. 10a is roughly hexagonal so its orientation is close to [1 0 0]. Orientation of the ceria particle can also be deduced thanks to the superstructure fringes seen on it. Such fringes are usually observed in reduced ceria along [1 1 0] direction and are perpendicular to (1 1 1) fringes, so the orientation of the ceria crystallite could be [−1 1 −2]. Therefore, the orientation relationship is: (1 1 1) CeO₂|| (0 0 2) Ru and [−1 1 −2] CeO₂|| [1 0 0] Ru. An example of strong superstructure fringes is shown in Fig. 10d for the Ce_{0.89}Ru_{0.11}O₂ reduced at 1000 °C, though they appeared already in the sample reduced at 600 °C (cf. Fig. 9c). Such superstructure fringes were observed previously in ceria based mixed oxides, e.g., Ce_{0.5}Yb_{0.5}O_{1.75} [43] and Ce_{0.5}Lu_{0.5}O_{1.75} [44] subjected to high temperature treatment in air [40]. It is believed that the reason of the superstructure formation is generation and ordering of oxygen vacancies in the ceria lattice. Comparison of the observed and simulated SAED patterns for Ce_{0.5}Yb_{0.5}O_{1.75} showed that the 12.5% of oxygen atoms was missing [43]. Similar superstructure was also observed for the reduced Pd/CeO₂ prepared in one step combustion method where Pd where dispersed in the ceria [45]. Two types of superstructure fringes were observed: 0.57 nm along [0 0 1]

direction and 0.8 nm along [−1 1 0] direction. The latter, similar to those observed in this work, were ascribed to ordering of point defects: O vacancies and Pd sites. Fig. 11 presents size distributions of Ru particles in the samples heated in hydrogen. Average size of Ru particles increased and the distributions broadened with increasing reduction temperature (Table 5). There is thus an apparent contradiction with XRD data where the reflections form Ru phase disappeared after reduction at high temperature (Fig. 8). There could be two reasons why Ru is not detected with XRD. First, the particles are too small (or they are too thin) to produce a strong Bragg reflections. And the second, that most of the particles are defected (have polytype structure – similar to that in Fig. 9d) what decreases the size of ordered domains below the detection limit of X-ray diffraction. As to the particle size it should be noted that in TEM images the Ru particles are represented mostly as 2D projections, so it is possible that particles appearing as relatively large in size are flat, and thus not detected by X-rays. The Ru particles formed at low temperature (500–600 °C) are small, but roughly hemispherical (Fig. 9c), while those formed at 1000 °C have bigger diameters but, interestingly, usually do not show crystal features (lattice fringes) (Fig. 10b). Most important observation is that despite severe reduction treatment (1000 °C,

Table 5
Average size of Ru and CeO₂ particles in Ce_{0.89}Ru_{0.11}O₂ heated in hydrogen.

	Average crystallite size [nm]				
	400 °C	500 °C	600 °C	800 °C	1000 °C
Ru (TEM)	n.o.	1.2 ± 0.3	1.3 ± 0.5	1.5 ± 1.2	2.2 ± 1.3
CeO ₂ (XRD)	6.8	15	26	36	60

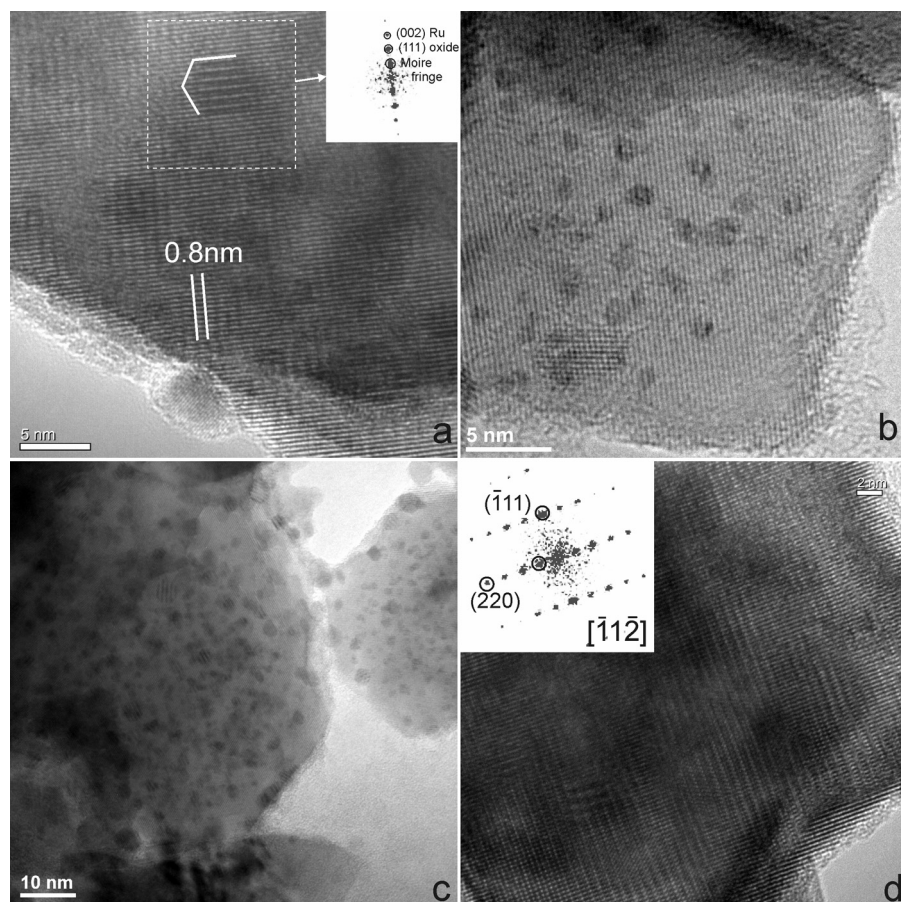


Fig. 10. TEM images of $\text{Ce}_{0.89}\text{Ru}_{0.11}\text{O}_2$ heated in hydrogen atmosphere at 1000°C : Ru crystallite with Moire fringes (a), flat Ru particles (b), low magnification general view (c), partly reduced ceria crystallite in $[-1 \ 1 \ -2]$ orientation (d).

3 h) growth of the mean crystallite size of Ru was small (Table 5). It proves a strong interaction of Ru with the surface of CeO_2 which, as we believe, manifests as epitaxial orientation. Epitaxial orientation was frequently observed for noble metals supported on CeO_2 and reduced in hydrogen atmosphere [42,46–49]. In the previous works, we observed formation of metal crystallites at the surface of the $\text{Ce}_{0.9}\text{NM}_{0.1}\text{O}_{2-y}$ ($\text{NM} = \text{Pd}, \text{Rh}$) reduced in hydrogen [21,22]. The particles exhibited preferred epitaxial orientation but contrary to Ru, a continuous growth of intensity of the metal reflections in XRD patterns was observed with increasing temperature of reduction. Similar to Ru, most of the Rh particles were small and epitaxially oriented at 1000°C but there was also a fraction of bigger 10–14 nm particles. The differences in behavior of Pd, Rh and Ru may be due to different crystal structure – fcc cubic or hexagonal, respectively, but also to difference in cohesion energy (melting point is 1555°C for Pd, 1964°C for Rh and 2334°C for Ru), which makes Ru less prone to sintering. Analysis of Fig. 8 and data in Table 5 shows that extensive sintering of ceria occurred during heating in hydrogen atmosphere. As the result a surface area of ceria decreases and it may be responsible for the growth of bigger Ru particles at the surface (5–10 nm). However, most of the ruthenium remains as very small 1–2 nm particles (Fig. 10b and c).

XPS also showed that the surface composition of the $\text{Ce}_{0.89}\text{Ru}_{0.11}\text{O}_2$ changed drastically after reduction at 800°C relative to the “as prepared” sample. Fig. 4c and 4g present high resolution XPS spectra of $\text{Ru}(3\text{d}_{5/2})$ and $\text{Ru}(3\text{p}_{3/2})$, respectively. Contrary to the single $\text{Ru}(3\text{p}_{3/2})$ line at 282.3 eV in the “as prepared” sample (Fig. 4f), after reduction at 800°C the line could be deconvoluted into 3 components at $279.8, 280.8$ and 282.3 eV (Fig. 4g, Table 2).

The first line corresponds well with metallic (neutral) Ru in Ru nanoparticles [27]. The second fits to RuO_2 oxide and the third to Ru ions in the $\text{Ce}_{0.9}\text{Ru}_{0.1}\text{O}_2$ mixed oxide. In a weaker, $\text{Ru}(3\text{p}_{3/2})$ line (Fig. 4c) two components could be defined: at 461.6 and at 462.9 eV . The former is close to the value for metallic Ru [34] and the latter, which is relatively broad, contains contributions from Ru^{4+} ions in RuO_2 and in $\text{Ce}_{0.9}\text{Ru}_{0.1}\text{O}_2$. The content of metallic Ru may be estimated from the intensities of the components as $I_{\text{Ru}1}/(I_{\text{Ru}1} + I_{\text{Ru}2}) = 0.56$. The remaining part of Ru is present as RuO_2 layer at the surface of Ru particles and as Ru^{4+} ions in the ceria lattice. These data can be interpreted as follows. During reduction treatment at 800°C most of the Ru escapes from the ceria lattice to the surface, where it forms Ru nanoparticles. After exposure to air the Ru particles undergo surface oxidation to RuO_2 what was

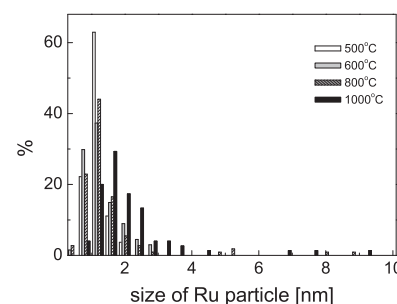


Fig. 11. Size distributions of Ru particles in $\text{Ce}_{0.89}\text{Ru}_{0.11}\text{O}_2$ reduced at various temperatures.

also visible on TEM image (Fig. 9c). Quantitative analysis of XPS spectra shows that reduction at 800 °C caused in addition to strong increase of Ru concentration a decrease of the O content at the surface (Table 3). The reduction process, which is known to bring also bulk reduction of ceria, increased, as expected, the ratio of Ce³⁺ in the sample. It should be remembered however, that a possibility of reoxidation of the sample reduced in hydrogen ($\text{Ce}_{0.89}\text{Ru}_{0.11}\text{O}_2$) after exposure to air as well as X-ray induced reduction of the samples during measurement make the quantitative results rather ambiguous.

3.1.4. Re-oxidation

$\text{Ce}_{0.89}\text{Ru}_{0.11}\text{O}_2$ sample reduced at 500 °C for 1 h (first reduction) was oxidized for 2 h at the same temperature. As the result, instead of very weak, broad reflections of Ru, sharp reflections from RuO_2 appeared in XRD pattern (Fig. S5). The amount of RuO_2 has been estimated as 2.5 wt.%. Next, the sample was again reduced at 500 °C for 1 h (second reduction) what caused the occurrence of well resolved reflections from metallic Ru. The amount of Ru has been estimated as 4 wt.% and the mean crystallite size as 17 nm, much bigger than that after the first reduction. It is clear therefore, that for the $\text{Ce}_{0.89}\text{Ru}_{0.11}\text{O}_2$ studied in this work, a self-regenerative property, observed previously for $\text{Ce}_{0.89}\text{Pd}_{0.11}\text{O}_{2-y}$ and $\text{Ce}_{0.89}\text{Rh}_{0.11}\text{O}_{2-y}$ [21,22], did not appear. The reason is probably relatively weak interaction of RuO_2 with the surface of doped ceria leading to its sintering. Quite different results were obtained by Satsuma et al. [39], who reported a self-dispersion of large Ru particles on the surface of CeO_2 during the oxidation treatment. This apparent contradiction may be due to a difference in the interaction of RuO_x species with the surface of pure cerium oxide and ceria highly doped with ruthenium. As was mentioned earlier, the abnormal growth of RuO_2 crystallites occurred during heating of $\text{Ce}_{0.89}\text{Ru}_{0.11}\text{O}_2$ in oxidizing atmosphere but not for Ru/ CeO_2 obtained by impregnation.

Singh and Hegde [13] observed fully reversible structure changes in $\text{Ce}_{0.89}\text{Ru}_{0.11}\text{O}_{2-y}$ upon reduction/oxidation cycle. In each cycle the sample was reduced up to 500 °C and then oxidized at 250 °C. H₂-TPR profiles were recurrent in every cycle and has very strong peak ~150 °C. The authors deduced from H₂ consumption that entire Ru in the lattice was reduced up to 500 °C and moreover Ru promoted cerium reduction. XRD patterns revealed that no crystalline Ru or RuO_2 was formed during the cycling. The contradiction between the results of [13] and ours may origin from differences in the sample preparation and treatment. Mean crystallite size of ceria obtained in the present work is 4 nm, much less than 10 nm in [13]. As the result we observed during the first reduction a noticeable and irreversible growth of the mean size of ceria to 15 nm and precipitation of small (1 nm) Ru particles. Moreover, we performed the re-oxidation treatment at 500 °C, i.e., at much higher temperature than 250 °C used in [13]. It should be mentioned that direct oxidation of $\text{Ce}_{0.89}\text{Ru}_{0.11}\text{O}_2$ at 500 °C ("as prepared" sample) did not cause segregation of RuO_2 (Fig. 1). It appears that Ru⁴⁺ ions are strongly bound in the ceria lattice. On the other hand, Ru–O species which forms as the result of oxidation of Ru particles at the surface of $\text{Ce}_{0.89}\text{Ru}_{0.11}\text{O}_2$, are mobile and aggregate into large RuO_2 crystallites.

3.2. Reduction – oxidation

3.2.1. H₂-TPR

Fig. 12 depicts H₂-TPR profiles for $\text{Ce}_{0.89}\text{Ru}_{0.11}\text{O}_2$ (a), 3%Ru/ CeO_2 (b) and CeO_2 (c). Three regions can be distinguished in the TPR profiles. A low temperature region below 200 °C, a middle temperature 200–500 °C and high temperature above 500 °C. The hydrogen consumptions in each region are given in Table 6. TPR profile of ceria (Fig. 12c) shows two wide maxima at 432 °C and 814 °C corresponding to surface and bulk reduction, respectively. The profile

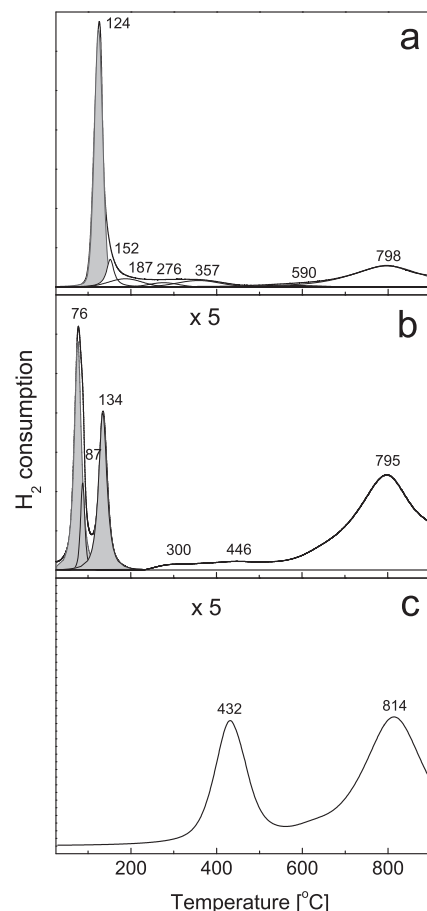


Fig. 12. H₂-TPR profiles of $\text{Ce}_{0.89}\text{Ru}_{0.11}\text{O}_2$ (a), 3%Ru/ CeO_2 (b) and CeO_2 (c). Note the 5× expansion of ordinate axes in (b) and (c).

of 3% Ru/ CeO_2 contains two strong maxima at 76 and 134 °C, then weak broad features centered at 300 and 446 °C and finally strong band at 795 °C. The low temperature maxima are assigned to the reduction of RuO_2 in highly dispersed or crystalline form, respectively [51]. The ratio of the maxima depends on the Ru loading but also on the temperature of calcination, with the second maximum increasing with these parameters. For low loadings (below 1.5 wt.% Ru) and/or low calcination temperature a single maximum is observed [51–54]. It is interesting that the maximum corresponding to a surface reduction of ceria is almost absent in the profile of 3 wt.% Ru/ CeO_2 . The reason could be a formation of (Ru–O–Ce) surface bonds during impregnation and calcination of the sample at 500 °C. Oxygen in such bonds is weakly bounded, and thus readily reduces at temperatures below 200 °C [51,53,54]. The high temperature maximum, corresponding to bulk reduction of ceria is slightly shifted toward lower temperatures. The profile of $\text{Ce}_{0.89}\text{Ru}_{0.11}\text{O}_2$ differs strongly from both CeO_2 and 3%Ru/ CeO_2 . In particular there is huge single maximum at 124 °C (note that the ordinate scale is multiplied by 5 in b and c), followed by weak broad features between 150 °C and 500 °C and relatively strong feature in high temperature region with maximum at 798 °C. The presence of a single maximum at 124 °C and lack of a maximum at ~70 °C, clearly show that the $\text{Ce}_{0.89}\text{Ru}_{0.11}\text{O}_2$ is structurally and chemically different from the 3%Ru/ CeO_2 prepared by impregnation. In particular it indicates that the surface of the mixed oxide is more homogeneous and more susceptible to reduction. High intensity of the maximum at 124 °C, much higher than expected for the reduction of the whole amount of Ru⁴⁺ present in the sample into Ru⁰, confirms that the surface reduction of Ce⁴⁺ into Ce³⁺ occurs already at such low

Table 6

Hydrogen uptake during the first TPR run.

Sample	H ₂ consumption [mmol/g]				Oxygen content
	Up to 200 °C	200–500 °C	500–900 °C	Total	
Ce _{0.89} Ru _{0.11} O ₂	1.66	0.77	1.1	3.53 (1.24) ^a	CeO _{1.58}
3 wt.% Ru/CeO ₂	0.56	0.09	0.92	1.57 (0.6) ^a	CeO _{1.82}
CeO ₂	–	0.72	1.23	1.95	CeO _{1.64}

^a H₂ consumption calculated for the complete reduction of Ru⁴⁺ to Ru⁰ (according to the reaction RuO₂ + 2H₂ = Ru + 2H₂O).

temperature. High temperature maximum at 798 °C, assigned to bulk reduction of ceria is similar to that for 3%Ru/CeO₂. The amount of H₂ consumed up to 200 °C was 1.66 mmol H₂ per gram of the sample (Table 6). Taking into account that the surface area of Ce_{0.89}Ru_{0.11}O₂ is 124 m²/g it gives 0.01328 mmol H₂/m². On the other hand, the most stable (1 1 1) surface of CeO₂ contains 15.8 O atoms per square nm in a top O—Ce—O trilayer, what gives 0.0262 mmol O/m². Since the stoichiometry of the reaction is H₂ + O = H₂O than roughly half oxygen atoms at the surface are removed up to 200 °C. Further reduction up to 900 °C consumes additional 1.87 mmol H₂/g, giving the total H₂ consumption of 3.53 mmol H₂/g. The hydrogen is used for complete reduction of Ru⁴⁺ to Ru⁰ (according to the reaction RuO₂ + 2H₂ = Ru + 2H₂O) and partial reduction of ceria to CeO_{1.58}. It is interesting to compare these results with those for bare CeO₂ nanoparticles. In this case the amount of H₂ consumed up to 500 °C was 0.72 mmol H₂ per gram of the sample (Table 6). Given that the surface area of CeO₂ is 62 m²/g it gives 0.0116 mmol H₂/m². Since there are 0.0262 mmol O/m² at the (1 1 1) surface of CeO₂ it appears that less than a half of oxygen atoms at the surface is removed up to 500 °C. It clearly shows strongly enhanced reducibility of the Ce_{0.89}Ru_{0.11}O₂ at low temperatures compared with pure CeO₂. The effect does not manifest at high temperatures because the H₂ consumption between 500 °C and 900 °C was similar (Table 6). Singh and Hegde [13] studied the reduction of Ce_{0.90}Ru_{0.10}O_{1.94} prepared by hydrothermal method. H₂-TPR profiles revealed that strong maximum of H₂ consumption occurs at ~125 °C and up to 500 °C the sample is reduced up to Ce_{0.90}Ru_{0.10}O_{1.52} [13]. The fact of deep reduction (60% of Ce³⁺) has been confirmed by thermogravimetry in hydrogen atmosphere. OSC estimated from H₂ consumption up to 500 °C in [13] was 0.464 and 2.512 mmol[O]/g for CeO₂ and Ce_{0.90}Ru_{0.10}O₂, respectively. In our case the corresponding values are: 0.552 and 1.448 mmol[O]/g, respectively. Much lower OSC for Ru doped ceria studied in this work is rather unexpected, given the similar Ru content and smaller crystallite size (4 nm versus 10 nm). The reason may be lower temperature of the sample pretreatment (120 °C vs. 500 °C) applied in [13]. Pretreatment at such low temperature may leave organic residues at the surface giving rise to H₂ consumption. In fact Ru 3d XPS spectrum of Ce_{0.90}Ru_{0.10}O_{1.94} presented in [13] shows huge peak from an adventitious carbon.

Sharma et al., [14] reported H₂-TPR profiles of nanocrystalline Ce_{0.95}Ru_{0.05}O₂ (~10 nm) prepared by a combustion method. The H₂ consumption started at 130 °C reaching a maximum at 200 °C and then it decreased slowly reaching almost zero at ~500 °C. An enhanced reducibility of the Ru doped ceria has been confirmed by DFT calculations [54]. The authors reported that activation energy of oxygen vacancy formation in Ce_{0.875}Ru_{0.125}O₂ (1.03 eV) is significantly lower than that in pure CeO₂ (3.2 eV). The reason is that substitution with noble metal ions activates lattice oxygen by creation of longer Ce—O and Ru—O bond lengths compared to those in CeO₂ and RuO₂ metal oxides. The calculations showed also that the (1 1 1) surface of Ce_{0.875}Ru_{0.125}O₂ should exhibit high activity in low temperature oxidation of CO [16]. The analysis of the charge distribution (the Bader charge calculations) revealed that in Ce_{0.875}Ru_{0.125}O₂ both Ru and Ce are in +4 oxidation state, while in the reduced oxide (with an oxygen vacancy) Ru ion close to

the vacancy remains in +4 state, while Ce⁴⁺ is reduced to +3 [16]. It explains why Ce_{0.89}Ru_{0.11}O₂ shows high structural stability in the reducing atmosphere, with a weak tendency to segregation of metallic Ru.

The second H₂-TPR profiles, obtained after completion of the first TPR run followed by re-oxidation up to 500 °C (TPO experiment—see below), of Ce_{0.89}Ru_{0.11}O₂ and 3 wt.% Ru/CeO₂ were similar (Fig. S6). In both there are series of close lying peaks below 250 °C with a maximum at ~120 °C, followed with broad feature between 250 °C and 500 °C. The reason of such behavior is mainly a structure change occurring in Ce_{0.89}Ru_{0.11}O₂ during the first TPR – run, namely reduction of Ru and its segregation at the surface of ceria as small metal particles. Upon oxidation step Ru oxidizes but remains at the surface, so that microstructure of both samples became similar. Bigger consumption of hydrogen by the Ce_{0.89}Ru_{0.11}O₂ up to 500 °C is due to higher Ru content and the fact that small amount of Ru ions could still be present in the ceria lattice.

3.2.2. O₂-TPO

O₂-TPO profiles of the samples were acquired after completion of the first TPR-run. When analyzing the profiles it should be considered that noticeable oxidation of the samples may occur before the onset of the profile acquisition (e.g., during switching the gas atmosphere). Oxidation profiles of CeO₂ (c) and 3 wt.% Ru/CeO₂ (b) are similar and contain a single peak below 100 °C, which can be assigned to oxidation of remaining Ce³⁺ (Fig. S7 supporting information). The profile of Ce_{0.89}Ru_{0.11}O₂ is completely different, since noticeable amount of O₂ is consumed almost continuously up to 500 °C. This result is consistent with TEM data for the Ce_{0.89}Ru_{0.11}O₂ reduced at high temperature, which showed superstructure fringes due to ordered oxygen vacancies. Such partially reduced oxide is stable in air at room temperature (sample for TEM was prepared ex situ) and clearly its oxidation is an activated process. It is possible also that the stability of the reduced oxide may be promoted by Ru ions present in the ceria lattice.

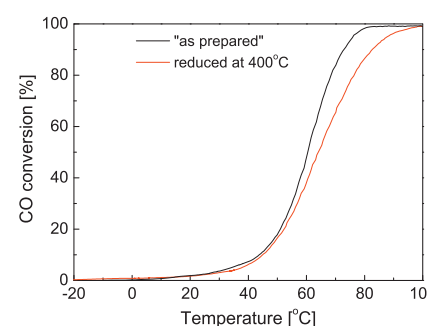


Fig. 13. CO conversion as a function of temperature over the Ce_{0.89}Ru_{0.11}O₂: “as prepared” (a) and reduced at 400 °C in H₂ (b).

3.3. Catalytic performance

3.3.1. CO oxidation

Fig. 13 presents temperature dependence of CO conversion to CO₂ in two runs on the “as-prepared” Ce_{0.89}Ru_{0.11}O_{2-y} sample. After the first run the sample was reduced “in situ” in the reactor in 5% H₂/Ar flow (50 ml/min) up to 400 °C with a heating rate 10 °C/min. Then it was cooled down to –20 °C in hydrogen, outgassed and flushed with pure He. In the first run CO oxidation starts at room temperature and increases steeply reaching 100% conversion at 85 °C. In the second run activity of the sample is slightly lower attaining 100% conversion at 100 °C. Two interesting facts appear from above results. The first is that the “as prepared” Ce_{0.89}Ru_{0.11}O_{2-y} shows very high activity in CO oxidation without any pretreatment. According to XPS, the Ru(3d_{5/2}) line of the “as prepared” Ce_{0.89}Ru_{0.11}O₂ (**Fig. 4f**) contains only one component at 282.3 eV, at energy even higher than that of RuO₂, excluding the presence of metallic Ru. HRTEM and XRD also confirmed that the sample is a single phase mixed oxide. Moreover, H₂-TPR profile of the “as prepared” Ce_{0.89}Ru_{0.11}O₂ shows no evidence of Ru reduction below 100 °C (**Fig. 12a**). These results apparently indicate that the oxidized form of Ru, as Ru⁴⁺ ions substituting Ce⁴⁺ in the ceria lattice, is an active phase in CO oxidation, unless it is assumed that Ru reduction occurs at low temperature during the catalytic test. As evidenced by the second run, the pre-reduction of Ce_{0.89}Ru_{0.11}O₂ at 400 °C did not change the initial activity at low temperatures but worsened slightly the activity at higher temperatures (a 100% conversion was attained at 100 °C). Such behavior confirms that ionic Ru participates in low temperature CO oxidation and is in strong contradiction with that observed for Ce_{0.89}Pd_{0.11}O_{2-y}, where pre-reduction in H₂ at 400 °C strongly enhanced the activity in CO combustion [21]. The reason is that, contrary to Ce_{0.89}Pd_{0.11}O_{2-y}, pre-reduction of Ce_{0.89}Ru_{0.11}O_{2-y} at 400 °C did not cause any drastic change in the microstructure (phase separation), but only a 50% growth of the mean crystallite size of ceria (**Fig. 8**, **Table 5**, **Fig. S4**). The effect of extensive surface reduction during exposure to H₂ at temperature up to 400 °C, evidenced by H₂-TPR (**Fig. 12a**), is probably reversed by an exposure of the sample to CO + artificial air reaction mixture at low temperature. In fact a momentary rise of the temperature of the sample was detected after the switching process from He to the reaction mixture in the second reaction run. In harmony with our data, a low temperature CO combustion (100% conversion at 105 °C) was reported over nanocrystalline Ce_{0.9}Ru_{0.1}O_{1.95} (8–10 nm) prepared by the hydrothermal method [13]. Interestingly, even without feed of oxygen, 60% CO conversion was achieved at 130 °C. These observations, as well as recent DFT calculations [16], confirm that Ru substitution in ceria effectively activate lattice oxygen to enable its extraction at low temperatures. On the contrary, for RuO₂ highly dispersed on CeO₂, pre-reduction in H₂ at 400 °C was necessary to increase the CO conversion at 100 °C from 15 to 40% [36].

3.3.2. Soot combustion

Activity of Ce_{0.89}Ru_{0.11}O₂ as an oxidizing catalyst was also checked in a model reaction of soot combustion. **Fig. 14** shows the TG profile representing the catalytic soot oxidation in air. The profile is compared with those obtained for bare soot and the soot mixed with nanocrystalline CeO₂ and Ce_{0.89}NM_{0.11}O_{2-y} (NM = Pd, Rh), which were synthesized using the same microemulsion method. **Table 7** presents values of initial (T_i) and final (T_f) temperature of soot combustion and also the temperature when half of the soot has been combusted ($T_{1/2}$). It appears that Ce_{0.89}Ru_{0.11}O₂ is the most active catalyst with $T_{1/2} = 398$ °C, ~15 °C lower than that of Pd or Rh doped ceria, 50° lower than for undoped ceria and 200 °C lower than for bare soot. An initial sample weight loss observed below 300 °C for all samples containing ceria was attributed to

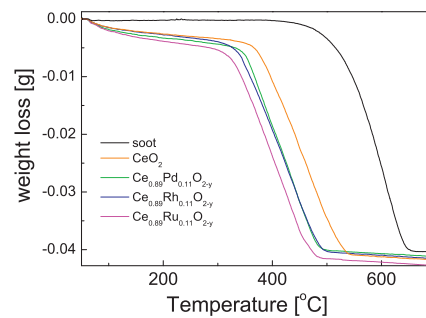


Fig. 14. TG curves of soot combustion in air catalyzed by nanocrystalline CeO₂, Ce_{0.89}Pd_{0.11}O_{2-y}, Ce_{0.89}Rh_{0.11}O_{2-y} and Ce_{0.89}Ru_{0.11}O₂.

Table 7
Soot oxidation in air in TGA.

Catalyst	T_i [°C]	$T_{1/2}$ [°C]	T_f [°C]
–	395	584	662
CeO ₂	323	449	542
Ce _{0.89} Pd _{0.11} O _{2-y}	312	415	501
Ce _{0.89} Rh _{0.11} O _{2-y}	293	412	506
Ce _{0.89} Ru _{0.11} O ₂	281	398	492

desorption of adsorbed species like water, carbonate group etc. The value $T_{1/2} = 398$ °C obtained in this work for Ce_{0.89}Ru_{0.11}O₂ is higher than $T_{1/2} = 350$ °C reported for oxidized Ru/CeO₂ catalyst [51]. These values are however hard to be compared because of different carbon/catalyst ratio used: 1:2 [this work] vs. 1:4 [51]. There are two properties of Ce_{0.89}Ru_{0.11}O₂ that make it active catalyst of soot oxidation. First is high ability to deliver oxygen from the lattice (reducibility) over broad temperature range from 80 to 500 °C (**Fig. 12a**), which according to a general agreement determines the effectiveness of the catalyst in the soot oxidation ([55] and references therein). According to literature, ceria based mixed oxides posses such ability and are active in soot combustion [56–59]. For nanocrystalline Ce_{0.75}Zr_{0.25}O₂ and Ce_{0.95}Fe_{0.05}O_{1.975} and soot/catalyst ratio 1:20, $T_{1/2} = 387$ °C and 366 °C, respectively was reported [58]. Nanocrystalline cerium oxides doped with lanthanides (Y, Pr, Tb, Lu) [57,59] gave $T_{1/2} = 480$ –530 °C. A direct comparing of the activities expressed as $T_{1/2}$ may be however misleading because experimental conditions such as ratio of the catalyst to soot and contact between them (loose or tight) strongly effect this parameter [60]. Another characteristic of Ce_{0.89}Ru_{0.11}O₂, important to its potential application for the soot oxidation, is a high surface area and structural and chemical stability in both oxidation and reducing atmospheres at temperature of the reaction (280–500 °C). The addition of Ru allows synthesizing the ceria based material with small crystallite size but also hinders the sintering of ceria at higher temperatures thus preserving the high surface area.

4. Conclusions

Nanocrystalline, Ce_{1-x}Ru_xO₂ mixed oxides, chemically homogeneous for x up to 0.13, with narrow size distribution and average size 3–5 nm were obtained using the microemulsion method. The Ce_{0.89}Ru_{0.11}O₂ oxide remained a single phase up to 550 °C in oxygen atmosphere, but at 600 °C a phase separation occurred suddenly with formation of large (0.2–1 μm) RuO₂ crystals. Similar effect was observed in argon atmosphere, but at temperature 100 °C higher. No phase separation was observed for Ce_{0.97}Ru_{0.03}O₂ even after heating at 800 °C. For Ru/CeO₂ samples prepared by impregnation, calcination at 800 °C caused almost complete spreading of Ru over CeO₂ for 3 wt.% Ru loading but only partial spreading for 8 wt.% Ru loading. Taking into account the surface area of CeO₂ support, it

appears that maximum ca. 5 Ru atoms/nm² may be involved in Ru–O–Ce surface phase stable at 800 °C in oxidizing atmosphere. The surplus Ru oxide is only weakly bound with the surface and sinters easily to form large RuO₂ crystallites. Doping with Ru decreases the size of ceria particles and strongly hinders their sintering at high temperatures. In hydrogen atmosphere the segregation of small ~1 nm Ru particles occurred at 500 °C. Increasing the reduction temperature up to 1000 °C had very little effect on the particle size of Ru, which indicates a very strong interaction of Ru with the surface of CeO₂. Contrary to other noble metals (e.g., Pd or Rh) the Ru–CeO₂ interaction did not weaken with temperature and even at 1000 °C small ruthenium particles were epitaxially orientated on ceria with Ru (002)||CeO₂ (111). Differently than in oxidizing atmosphere, doping with Ru had no significant effect on the sintering of ceria in hydrogen.

Nanocrystalline Ce_{1-x}Ru_xO₂ exhibits strongly enhanced reducibility at low temperatures as compare to pure CeO₂. H₂-TPR indicates that half of oxygen atoms at the surface are removed up to 200 °C, while for nanocrystalline CeO₂ a quarter of oxygen atoms at the surface is removed between 300 °C and 500 °C. The susceptibility of Ce_{0.89}Ru_{0.11}O₂ to release oxygen results in its high activity in CO and soot oxidation.

Acknowledgements

This work was financially supported by the National Science Center in Poland (grant 2011/01/N/ST5/05609). The authors thank Dr. A. Gagor and Mrs. E. Bukowska for XRD work. MK thanks Dr. M.G. Willinger of Microscopy Group in Fritz Haber Institute of the Max Planck Society for giving a possibility to use TEM/STEM instrument.

Appendix A. Supplementary data

Supplementary data associated with this article can be found, in the online version, at <http://dx.doi.org/10.1016/j.apcatb.2013.10.047>.

References

- [1] M.S. Hegde, G. Madras, K.C. Patil, *Acc. Chem. Res.* 42 (2009) 704–712.
- [2] A. Gupta, U.V. Waghmare, M.S. Hegde, *Chem. Mater.* 22 (2010) 5184–5198.
- [3] D.O. Scanlon, B.J. Morganand, G.W. Watson, *Phys. Chem. Chem. Phys.* 13 (2011) 4279–4284.
- [4] R. Rangel, L. Chavez-Chavez, E. Martinez, P. Bartolo-Perez, *Phys. Status Solidi B* 249 (2012) 1199–1205.
- [5] Z. Hu, H. Metiu, *J. Phys. Chem. C* 115 (2011) 17898–17909.
- [6] L. Oliviero, J. Barbier Jr., D. Duprez, A. Guerrero-Ruiz, B. Bachiller-Baeza, I. Rodriguez-Ramos, *Appl. Catal. B: Environ.* 25 (2000) 267–275.
- [7] S. Imamura, Y. Taniguchi, Y. Ikeda, S. Hosokawa, H. Kanai, H. Ando, *React. Kinet. Catal. Lett.* 76 (2002) 201–206.
- [8] J. Barbier Jr., L. Oliviero, B. Renard, D. Duprez, *Top. Catal.* 33 (2005) 77–86.
- [9] S. Yang, Y. Feng, J. Wan, W. Zhu, Z. Jiang, *Appl. Surf. Sci.* 246 (2005) 222–228.
- [10] T. Abe, M. Tanizawa, K. Watanabe, A. Taguchi, *Energy Environ. Sci.* 2 (2009) 315–321.
- [11] L. Oliviero, J. Barbier Jr., S. Labruquere, D. Duprez, *Catal. Lett.* 60 (1999) 15–19.
- [12] S. Hosokawa, Y. Hayashi, S. Imamura, K. Wada, M. Inoue, *Catal. Lett.* 129 (2009) 394–399.
- [13] P. Singh, M.S. Hegde, *Chem. Mater.* 21 (2009) 3337–3345.
- [14] S. Sharma, Z. Hu, P. Zhang, E.W. McFarland, H. Metiu, *J. Catal.* 278 (2011) 297–309.
- [15] P. Singh, N. Mahadevaiah, S.K. Parida, M.S. Hegde, *J. Chem. Sci.* 123 (2011) 577–592.
- [16] H.T. Chen, *J. Phys. Chem. C* 116 (2012) 6239–6246.
- [17] M.A. Malecka, L. Kepinski, W. Mista, *J. Alloys Comp.* 451 (2008) 567–570.
- [18] M.M. Natile, A. Glisenti, *Surf. Sci. Spectra* 13 (2006) 17.
- [19] R.V. Gulyaev, L.S. Kibis, O.A. Stokus, A.V. Zadesenets, P.E. Plyusnin, Yu V. Shubin, S.V. Korenev, A.S. Ivanova, E.M. Slavinskaya, V.I. Zaikovskii, I.G. Danilova, A.I. Boronin, V.A. Sobyanin, *J. Struct. Chem.* 52 (2011) 123–136.
- [20] M. Kurnatowska, L. Kepinski, W. Mista, *Appl. Catal. B: Environ.* 117–118 (2012) 135–147.
- [21] M. Kurnatowska, L. Kepinski, *Mater. Res. Bull.* 48 (2013) 852–862.
- [22] XPSPEAK.41 program [R.W.M. Kwok].
- [23] E. Paparazzo, G.M. Ingo, N. Zaccetti, *J. Vac. Sci. Technol. A* 9 (1991) 1416.
- [24] L.J. Atanasoska, W.E. O'Grady, R.T. Atanasoski, F.H. Pollak, *Surf. Sci.* 202 (1988) 142–166.
- [25] S. Bhaskar, P.S. Dabal, S.B. Majumder, R.S. Katiyara, *J. Appl. Phys.* 89 (2001) 2987.
- [26] K. Qadir, S.H. Joo, B.S. Mun, D.R. Butcher, J.R. Renzas, F. Aksoy, Z. Liu, G.A. Somorjai, J.Y. Park, *Nano Lett.* 12 (2012) 5761–5768.
- [27] H. Over, A.P. Seitsonen, E. Lundgren, M. Smedh, J.N. Andersen, *Surf. Sci.* 504 (2002) 196.
- [28] P.A. Cox, J.B. Goodenough Cox, P.J. Tavener, D. Telles, R.G. Edgell, *J. Solid State Chem.* 62 (1986) 360.
- [29] H.J. Lewerenz, *Surf. Sci.* 126 (1983) 463–468.
- [30] Y. Kaga, Y. Abe, H. Yanagisawa, M. Kawamura, K. Sasaki, *Surf. Sci. Spectra* 6 (1999) 68.
- [31] J. Okal, M. Zawadzki, W. Tylus, *Appl. Catal. B: Environ.* 101 (2011) 548–559.
- [32] H. Over, *Chem. Rev.* 112 (2012) 3356–3426.
- [33] M.A. Ernst, W.G. Sloof, *Surf. Interface Anal.* 40 (2008) 334–337.
- [34] J.Y. Shen, A. Adnot, S. Kaliaguine, *Appl. Surf. Sci.* 51 (1991) 47.
- [35] V.M. Shinde, G. Madras, *Appl. Catal. B: Environ.* 138–139 (2013) 51–61.
- [36] A.A. Bolzan, C. Fong, B.J. Kennedy, C.J. Howard, *Acta Crystallogr. B* 53 (1997) 373–380.
- [37] I.L. Chen, T.Y. Chen, C.C. Hu, C.H. Lee, *J. Mater. Chem. A* 1 (2013) 2039–2049.
- [38] A. Satsuma, M. Yanagihara, J. Ohyama, K. Shimizu, *Catal. Today* 201 (2013) 62–67.
- [39] L. Dong, Y. Chan, *J. Chem. Soc. Faraday Trans.* 92 (1996) 4589–4593.
- [40] L. Xiaowei, S. Mingmin, H. Xi, Z. Haiyang, G. Fei, K. Yan, D. Lin, C. Yi, *J. Phys. Chem. B* 109 (2005) 3949–3955.
- [41] J.C. Hernandez, S. Trasobares, J.M. Gatica, D.M. Vidal, M.A. Cauqui, J.J. Calvino, A.B. Hungria, J.A. Perez-Omil, *EMC 2008*, vol. 2: *Mater. Sci.*, 2008, pp. 213–214.
- [42] M.A. Malecka, L. Kepinski, M. Maczka, *J. Solid State Chem.* 181 (2008) 2306–2312.
- [43] M.A. Malecka, L. Kepinski, *J. Microsc.* 237 (2010) 391–394.
- [44] S. Colussi, A. Gayen, M.F. Camellone, M. Boaro, J. Llorca, S. Fabris, A. Tovarelli, *Angew. Chem. Int. Ed.* 48 (2009) 8481–8484.
- [45] S. Bernal, F.J. Botana, J.J. Calvino, G.A. Cifredo, J.A. Perez-Omil, J.M. Pintado, *Catal. Today* 23 (1995) 219–250.
- [46] A.I. Boronin, E.M. Slavinskaya, I.G. Danilova, R.V. Gulyaev, Y.I. Amosov, P.A. Kuznetsov, I.A. Polukhina, S.V. Koscheev, V.I. Zaikovskii, A.S. Noskov, *Catal. Today* 144 (2009) 201–211.
- [47] L. Kepinski, M. Wolcyrz, *Appl. Catal. A: Gen.* 150 (1997) 197–220.
- [48] S. Bernal, G. Blanco, J.J. Calvino, C. López-Cartes, J.A. Perez-Omil, J.M. Gatica, O. Stephan, C. Colliex, *Catal. Lett.* 76 (2001) 3–4.
- [49] S. Aouad, E. Abi-Aad, A. Aboukais, *Appl. Catal. B: Environ.* 88 (2009) 249–256.
- [50] S. Hosokawa, H. Kanai, K. Utani, Y. Taniguchi, Y. Saito, S. Imamura, *Appl. Catal. B: Environ.* 45 (2003) 181–187.
- [51] Q. Dai, S. Bai, Z. Wang, X. Wang, G. Lu, *Appl. Catal. B: Environ.* 126 (2012) 64–75.
- [52] K. Wada, S. Hosokawa, M. Inoue, *Catal. Surv. Asia* 15 (2011) 1–11.
- [53] E. Aneggi, C. de Leitenburg, A. Tovarelli, *Catal. Today* 118 (2012) 108–115.
- [54] M. Machida, Y. Murata, K. Kishikawa, D. Zhang, K. Ikeue, *Chem. Mater.* 20 (2008) 4489–4494.
- [55] M. Malecka, L. Kepinski, W. Mista, *Appl. Catal. B: Environ.* 74 (2007) 290–298.
- [56] E. Aneggi, C. de Leitenburg, G. Dolcetti, A. Tovarelli, *Catal. Today* 114 (2006) 40–47.
- [57] I. Atribak, A. Bueno-Lopez, A. Garcia-Garcia, *J. Mol. Catal. A* 300 (2009) 103–110.
- [58] B.R. Stanmore, J.F. Brilhac, P. Gilot, *Carbon* 39 (2001) 2247–2268.